Soluble VEGF isoforms are essential for establishing epiphyseal vascularization and regulating chondrocyte development and survival

Christa Maes,[1] Ingrid Stockmans,[1] Karen Moermans,[1] Riet Van Looveren,[1] Nico Smets,[1] Peter Carmeliet,[2] Roger Bouillon,[1] and Geert Carmeliet[1]

[1]Laboratory of Experimental Medicine and Endocrinology, Katholieke Universiteit Leuven, Leuven, Belgium
[2]The Center for Transgene Technology and Gene Therapy, Flanders Interuniversity Institute for Biotechnology, Katholieke Universiteit Leuven, Leuven, Belgium

VEGF is crucial for metaphyseal bone vascularization. In contrast, the angiogenic factors required for vascularization of epiphyseal cartilage are unknown, although this represents a developmentally and clinically important aspect of bone growth. The *VEGF* gene is alternatively transcribed into $VEGF_{120}$, $VEGF_{164}$, and $VEGF_{188}$ isoforms that differ in matrix association and receptor binding. Their role in bone development was studied in mice expressing single isoforms. Here we report that expression of only $VEGF_{164}$ or only $VEGF_{188}$ (in $VEGF^{188/188}$ mice) was sufficient for metaphyseal development. $VEGF^{188/188}$ mice, however, showed dwarfism, disrupted development of growth plates and secondary ossification centers, and knee joint dysplasia. This phenotype was at least partly due to impaired vascularization surrounding the epiphysis, resulting in ectopically increased hypoxia and massive chondrocyte apoptosis in the interior of the epiphyseal cartilage. In addition to the vascular defect, we provide in vitro evidence that the $VEGF_{188}$ isoform alone is also insufficient to regulate chondrocyte proliferation and survival responses to hypoxia. Consistent herewith, chondrocytes in or close to the hypoxic zone in $VEGF^{188/188}$ mice showed increased proliferation and decreased differentiation. These findings indicate that the insoluble $VEGF_{188}$ isoform is insufficient for establishing epiphyseal vascularization and regulating cartilage development during endochondral bone formation.

This article was published online in advance of the print addition. The date of publication is available from the JCI website, http://www.jci.org. *J. Clin. Invest.* **113**:188–199 (2004). doi:10.1172/JCI200419383.

Introduction

Until secondary ossification occurs during endochondral bone development, epiphyseal cartilage remains avascular due to the production of angiogenic inhibitors. As a result, the center of the epiphysis is hypoxic, and survival of these chondrocytes is dependent on anaerobic glycolysis regulated by hypoxia-inducible factor-1α (HIF-1α) (1, 2). When the chondrocytes differentiate into mature hypertrophic cells they produce angiogenic stimulators and attract metaphyseal blood vessels. Metaphyseal vascular invasion is associated with apoptosis of terminal hypertrophic chondrocytes and recruitment of osteoblasts and osteoclasts/chondroclasts, resulting in the replacement of mineralized cartilage with bone and marrow (3).

Metaphyseal vessels derive from the nutrient artery, and metaphyseal vascularization is regulated by several factors including VEGF produced by hypertrophic chondrocytes (3). VEGF is a potent stimulator of embryonic and adult vascularization (4) existing as multiple spliced isoforms, $VEGF_{120}$, $VEGF_{164}$, and $VEGF_{188}$ in mice ($VEGF_{121}$, $VEGF_{165}$, and $VEGF_{189}$ in humans) (5). $VEGF_{120}$ is diffusible, $VEGF_{188}$ avidly binds to the cell surface and extracellular matrix, and $VEGF_{164}$ combines these properties. All isoforms bind the receptors Flt-1 (VEGF receptor-1) and Flk-1 (VEGF receptor-2), whereas only $VEGF_{164}$ has been shown to bind neuropilin-1 (NRP-1) (6, 7). Vascularization and mineralization in the metaphysis of long bones was impaired by blocking VEGF (8) and by targeted inactivation of $VEGF_{164}$ and $VEGF_{188}$, leaving expression of only the soluble isoform $VEGF_{120}$ ($VEGF^{120/120}$ mice) (9, 10), showing the pivotal role of the (partly) matrix-bound VEGF isoforms in metaphyseal vascularization and primary ossification.

In contrast, the mechanisms governing epiphyseal vascularization and the formation of the secondary ossification centers of long bones have not been elucidated. The oxygen and nutrient supply of developing avascular cartilage is thought to depend largely on the elaborate

Received for publication July 2, 2003, and accepted in revised form November 11, 2003.

Address correspondence to: G. Carmeliet, Legendo, Onderwijs en Navorsing, Campus Gasthuisberg, Herestraat 49, B-3000, Leuven, Belgium. Phone: 32-16-345974; Fax: 32-16-345934; E-mail: geert.carmeliet@med.kuleuven.ac.be.

Conflict of interest: The authors have declared that no conflict of interest exists.

Nonstandard abbreviations used: hypoxia-inducible factor-1α (HIF-1α); neuropilin-1 (NRP-1); membrane-type 1 MMP (MT1-MMP); postnatal day (P); embryonic day (E); tartrate-resistant acid phosphatase (TRAP); paraformaldehyde (PF); core-binding factor 1 (Cbfa-1); Indian hedgehog (Ihh); parathyroid hormone-related protein (PTHrP); Patched (Ptc); PTH/PTHrP receptor (PPR); neuropilin-1 (NRP-1) recombinant murine (rm); quantitative RT-PCR (qRT-PCR); receptor activator of NF-κB (RANK); hypoxanthine transferase (HPRT).

epiphyseal vascular network overlying the cartilaginous surface (11, 12). Invasion of these vessels into the epiphyseal cartilage represents a critical early step in the development of the secondary ossification center (13–15). The membrane-type 1 MMP (MT1-MMP) is the only known molecular signal implicated in this process (16, 17). Yet, epiphyseal vascularization is clinically important since interference with the epiphyseal blood supply leads to dysfunction of proliferating chondrocytes associated with reduced longitudinal growth (18, 19), and epiphyseal growth defects secondary to ischemia have been described in children (20, 21).

In the present study we show that metaphyseal vascularization and ossification was normal in mice expressing exclusively $VEGF_{164}$ (*VEGF*$^{164/164}$ mice) or $VEGF_{188}$ (*VEGF*$^{188/188}$ mice), indicating that either of the matrix-associated VEGF isoforms can provide the signals required for metaphyseal development. In contrast, *VEGF*$^{188/188}$ mice demonstrated impaired vascularization surrounding the epiphysis, associated with aberrant hypoxia and massive apoptosis within the cartilage. In addition to this vascular defect, in vitro experiments revealed that chondrocyte proliferation and survival in response to hypoxia was altered in *VEGF*$^{188/188}$ hind limbs as compared with WT limbs. As a result, the formation of secondary ossification centers was impaired and the *VEGF*$^{188/188}$ mice showed dwarfism and severe knee joint dysplasia. These findings provide new insights in the regulation of long bone development by revealing the role of soluble VEGF isoforms in establishing the epiphyseal vascular network and implicating VEGF in the development and survival of chondrocytes.

Methods

Animals. Targeted mutagenesis to generate *VEGF*$^{164/164}$ and *VEGF*$^{188/188}$ mice was achieved by homologous and Cre/*lox P*–mediated site-specific recombination in ES cells. Targeting vectors consisted of cDNA containing the fused exons 4, 5, 7, and 8 (for $VEGF_{164}$) or 4–8 (for $VEGF_{188}$), as described in detail elsewhere (22). The age of mice was stated as postnatal day (P) or embryonic day (E), E0.5 being the morning a vaginal plug was observed after overnight mating. Experiments were conducted with the approval of the ethical committee of the Katholieke Universiteit Leuven.

Histology, immunohistochemistry, histomorphometry, and skeletal preparation. All the histological methods, skeletal preparation, Von Kossa, tartrate-resistant acid phosphatase (TRAP), and CD31 stainings have been described previously (9). For collagen II immunostaining, sections were digested with 0.025% pepsin in 0.2 N HCl for 15 minutes at 37°C, fixed in 4% paraformaldehyde (PF), and quenched in 50 mM of NH_4Cl before incubation with a mouse anti-collagen II mAb (Chemicon International, Temecula, California, USA) and a goat anti-mouse secondary Ab conjugated with fluorescein (F. Hoffmann LaRoche AG, Basel, Switzerland). KI67 immunostaining (Novocastra Laboratories Ltd., Newcastle, United Kingdom) was carried out according to a standard protocol. Histomorphometric analysis was done using a Kontron Electronik (Eching bei München, Germany) image-analyzing system (KS400 V 3.00) (see ref. 9 and Supplementary data, http://www.jci.org/cgi/content/full/113/2/188/DC1).

Angiography. Neonatal pups were perfused through the left ventricle with 1.25% FITC-labeled dextran (mol wt. 2,000,000) (Sigma-Aldrich, St. Louis, Missouri, USA) containing 2.5% gelatin (50 μl/g body weight), outflow being enabled by opening the right atrium. Following the procedure, the hind limbs were dissected, fixed with 1% PF overnight, and stored in PBS at 4°C. After removal of the patella, the vascular network upon the epiphyseal condyles was readily visualized, contrasting the avascularity of the patellar face (*facies patellaris*) (see Figure 2g, anterior view of angiography). Epiphyseal vascular density was quantified by determining the percentage of vascularized surface of a defined area of the medial and lateral femoral condyles, encompassing approximately 0.5 mm^2, as illustrated in Figure 2g (boxed area).

BrdU incorporation. Pregnant females and P1.5 mice were injected intraperitoneally with 150 μg/g body weight BrdU (Sigma-Aldrich) 2.5 hours before sacrifice. Hind limbs were processed for paraffin embedding. Sections were incubated overnight with rat anti-BrdU Ab (Harlan Sera-Lab Ltd., Loughborough, United Kingdom), followed by a biotinylated rabbit anti-rat Ab (DAKO A/S, Glostrup, Denmark) and detection using avidin-biotin-peroxidase (ABC) complex (DAKO A/S). Sections were counterstained with light green or hematoxylin. The percentage of proliferating cells was determined as ratio of the number of BrdU-positive cells over the total number of cells, counted in defined areas as indicated.

EF5 distribution and TUNEL assay. Pregnant females and P1.5 mice were injected intraperitoneally with 10 mM EF5 (C. Koch, University of Pennsylvania, Philadelphia, Pennsylvania, USA, and the Cancer Therapy Evaluation Program, National Cancer Institute, Bethesda, Maryland, USA) at 1% of body weight. Three hours later, hind limbs were dissected, fixed in 4% PF for 2 hours, incubated overnight in 30% sucrose, and embedded in OCT. Frozen sections were cut (10 μm) and stained for EF5 as described (23). TUNEL assay was performed on frozen sections using In Situ Cell Death Detection Kit (F. Hoffmann LaRoche AG).

In situ hybridization. In situ hybridization was performed on paraffin sections as described (9) using riboprobes labeled with ^{35}S for collagen II, collagen X, or core-binding factor 1 (Cbfa-1/Runx-2) (see ref. 9), Indian hedgehog (Ihh), parathyroid hormone-related protein (PTHrP), Patched (Ptc), and PTH/PTHrP receptor (PPR) (from U.I. Chung, Massachusetts General Hospital, Boston, Massachusetts, USA), Flk-1 (C.J.M. de Vries, University of Amsterdam, Amsterdam, The Netherlands), and NRP-1 (J. Helms, University of

California, San Francisco, California, USA). Probes for Flt-1 (bp 900–1050) or exon 2–5 of VEGF (bp 94–429), recognizing all isoforms, were generated by standard cloning techniques. Pictures of hybridization signals were taken using a red filter and superimposed with bright-field images of the hematoxylin-stained tissues using a Zeiss Axioplan 2 microscope (Carl Zeiss, Jena GmbH, Jena, Germany) and KS400 V 3.00 and Adobe Photoshop software (Adobe Systems Inc., Mountain View, California, USA).

Primary chondrocyte cultures. Primary growth plate chondrocytes were isolated from the proximal tibia and distal femur of 10-day-old mice by collagenase digestion as described (24). Pooled chondrocytes from six animals were resuspended and cultured in six-well dishes (300,000 cells/well) in DMEM/F12 (1:1) medium (Life Technologies Inc., Paisley, Scotland, United Kingdom) supplemented with penicillin and streptomycin, 10% FCS, 50 μg/ml ascorbic acid, and 100 μg/ml sodium pyruvate. After overnight incubation in standard conditions, medium was refreshed and cells were incubated for 24 hours in normoxia (normal oxygen: 21% O_2) or hypoxia (0.5% O_2). Cell lysates were obtained with RNeasy lysis buffer (QIAGEN/Westburg BV, Leusden, The Netherlands) containing 1% β-mercaptoethanol.

Limb cultures. Hind limbs (tibia and femur) were dissected from E16.5 embryos, stripped of skin and surrounding tissues, and cultured overnight on a Falcon insert membrane (pore size 0.4 μm) in 12-well plates in BGJb medium (Life Technologies Inc.) supplemented with 0.1% BSA, 25 μg/ml ascorbic acid, and 10 mM β-glycerophosphate. Medium was then replaced, and culture was continued in normoxia (21% O_2) or hypoxia (0.5% O_2). For RNA analysis, limbs were snap-frozen in liquid nitrogen 24 hours later. For TUNEL and KI67 staining, limbs were cultured for 48 hours with or without 10 ng/ml recombinant murine (rm) $VEGF_{164}$ (N. Mertens, Flanders University Institute for Biotechnology, Ghent University, Ghent, Belgium) and processed to obtain frozen sections.

Isolation of RNA and quantitative RT-PCR. Total RNA from snap-frozen P1.5 femurs (n = 12) or cultured limbs (n = 5 per group) was extracted with TRIZOL (Life Technologies Inc.). RNA from cultured chondrocytes was extracted using RNeasy Mini Kit (QIAGEN/Westburg BV).

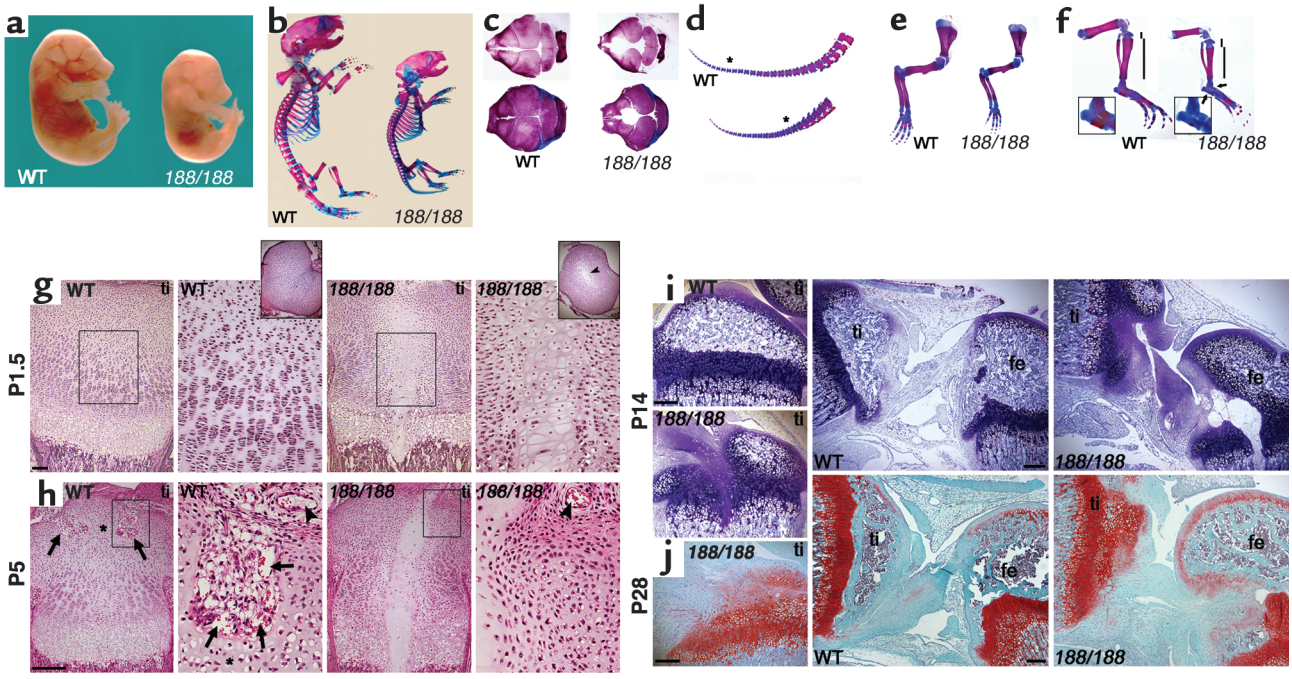

Figure 1

Abnormal bone, cartilage, and joint development in *VEGF*$^{188/188}$ mice. (**a**) Lateral view of WT and *VEGF*$^{188/188}$ (*188/188*) embryos at E16.5. (**b**) Skeletal preparation of pups at P1.5. (**c**) Calvaria at P1.5 (top) and P5 (bottom), showing delayed bone growth in the mutants. (**d**) P1.5 tails, showing reduced size and ossification in *VEGF*$^{188/188}$ mice. Asterisks indicate the most distal vertebrae with ossified center. (**e**) Forelimbs and (**f**) hind limbs at P1.5. Note incomplete ossification in talus and calcaneus (arrows and insets) and decreased length of the ossified diaphysis, but increased cartilage length in *VEGF*$^{188/188}$ bones (bars in **f**). (**g**–**j**) Histological analysis of epiphyseal cartilage of WT and *VEGF*$^{188/188}$ mice, showing sections through the center of proximal tibia (ti) and/or distal femur (fe). (**g**) H&E staining at P1.5, showing large hypocellular region in mutant cartilage. Higher magnification of the boxed area demonstrates abnormal cellular and nuclear morphology. Insets show transverse epiphysis sections, illustrating the restricted central localization of the defect (arrowhead). (**h**) H&E staining at P5. Asterisks indicate foci of hypertrophied epiphyseal chondrocytes, and arrows point at cartilage invasion by vascular canals in WT. Both features are absent in the mutants, where only perichondrial vessels (arrowhead) are seen adjacent to the cartilage. (**i**) P14 (toluidine blue) and (**j**) P28 (safranine O) tibia (left panel) and knee joint (right panels). Note strongly impaired formation of secondary ossification centers, extensive fibrosis and overgrowth of joint ligament tissues, and disruption of articular cartilage surfaces in *VEGF*$^{188/188}$ mice. Scale bars: (**g**) 100 μm; (**h**–**j**) 250 μm.

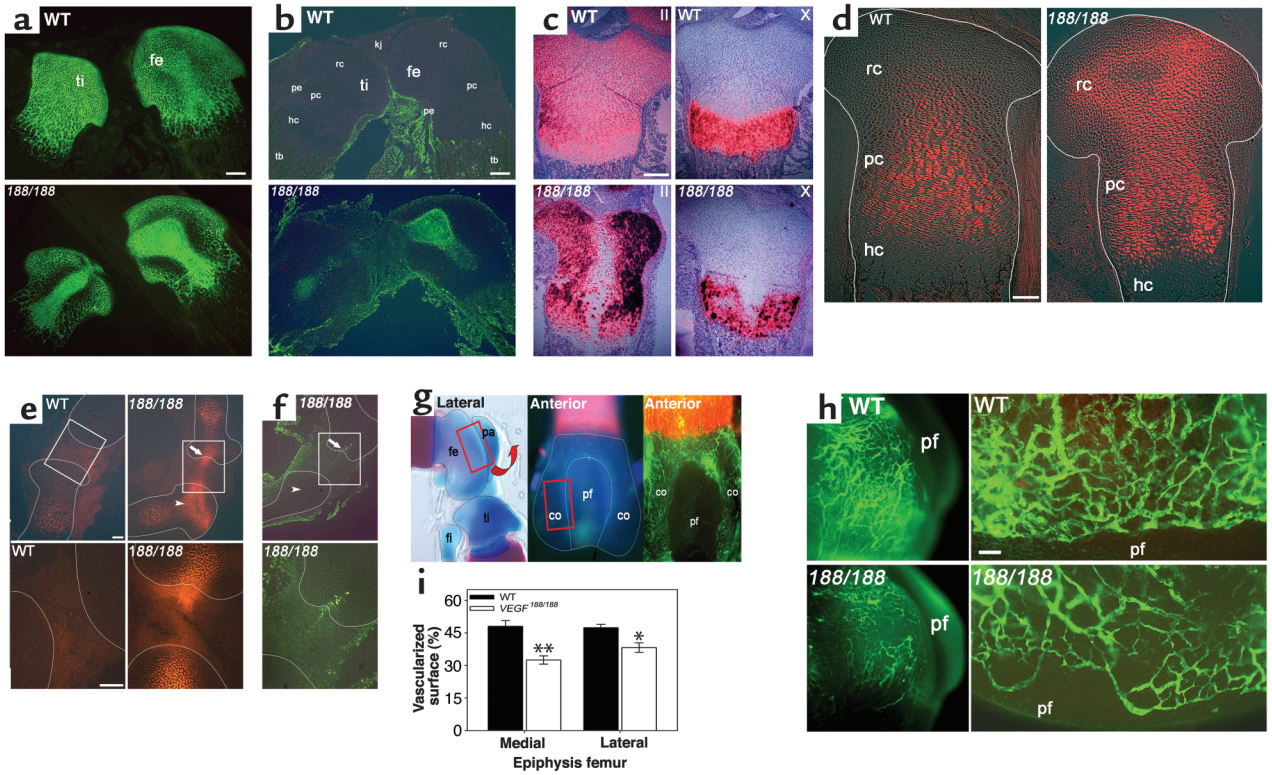

Figure 2

Central epiphyseal cartilage defects in *VEGF*$^{188/188}$ mice. (**a**–**c**) Central sections through WT and *VEGF*$^{188/188}$ (*188/188*) tibia/femur at P1.5. (**a**) Collagen II immunostaining shows its accumulation centrally in *VEGF*$^{188/188}$ cartilage. (**b**) TUNEL analysis detecting centrally localized apoptotic cells only in *VEGF*$^{188/188}$ epiphyses. (**c**) In situ hybridization fails to detect collagen II and collagen X mRNA in the center of mutant bones. (**d** and **e**) Hypoxia imaging by EF5 binding. (**d**) E18.5 distal femurs, showing strongly increased and ectopic hypoxia in mutant cartilage. (**e**) E16.5 knee joint and adjacent epiphyses (top panel) and magnification of the boxed area (lower panel). Note highly increased EF5 staining in the mutant bones, especially in resting/periarticular cartilage (arrowhead) and extending into the joint (arrow). (**f**) TUNEL staining detects an apoptotic cell cluster in the region of increased articular EF5 staining (arrow) in the mutants, whereas the epiphyseal cartilage itself is viable (arrowhead). (**g** and **h**) Angiography. (**g**) Lateral and anterior views of distal femur (skeletal staining or angiography), localizing the area of investigation and quantification (boxed area). (**h**) Low (left) and high (right) magnification of angiographies, showing the epiphyseal vessel network. Vessels appear thinner and more randomly orientated along the condylar rim in *VEGF*$^{188/188}$ mice compared with WT, and vascular density on the medial and lateral condyles is reduced. (**i**) ($n = 3$; $^*P < 0.05$; $^{**}P < 0.01$). Scale bars: (**a**–**c**) 200 μm; (**d**–**f**) 100 μm; (**h**) 50 μm. Kj, knee joint; rc, resting/periarticular cartilage; pc, proliferating/columnar chondrocytes; hc, hypertrophic cartilage; pe, perichondrium; tb, trabecular bone; fe, femur; ti, tibia; fi, fibula; pa, patella; co, condyle; pf, patellar face.

Quantitative RT-PCR (qRT-PCR) was performed as described (9), using specific primers and probes for Ihh, PTHrP, MMP-13, MT1-MMP, receptor activator of NF-κB (RANK), HIF-1α, HIF-2α, $VEGF_{164}$, $VEGF_{188}$, Flt-1, Flk-1, NRP-1, $VEGF_{120}$, total VEGF, Cbfa-1, osteocalcin, MMP-9, Bcl-2, and Bax (see Supplementary data, http://www.jci.org/cgi/content/full/113/2/188/DC1). Expression levels were normalized for hypoxanthine transferase (HPRT) expression.

Statistical analysis. Comparison between quantitative data of two groups was done by two-sided, two-sample Student *t* tests using NCSS (Kaysville, Utah, USA) software, and these data are expressed as mean plus or minus SEM. Significant differences are indicated as *P* values less than 0.05, 0.01, and 0.001. Multiple groups were analyzed by ANOVA followed by Fisher's least significant difference multiple-comparison test and shown as mean plus or minus SE. Significance was accepted at *P* values less than 0.05.

Results

Reduced growth and skeletal development of VEGF$^{188/188}$ *but not of VEGF*$^{164/164}$ *mice*. The growth and body weight of *VEGF*$^{164/164}$ mice was normal, and their skeleton had normal size, structure, and mineralization at P1.5 (not shown). In contrast, *VEGF*$^{188/188}$ mice were considerably smaller and had reduced body weights throughout embryonic and postnatal life as compared with WT animals (Figure 1a and Supplementary Figure 1a, http://www.jci.org/cgi/content/full/113/2/188/DC1). Strongly reduced size and mineral content of all skeletal elements was observed in *VEGF*$^{188/188}$ neonates (Figure 1b). Growth of the frontal and parietal bones was delayed (Figure 1c), vertebrae were smaller, and tail mineralization was strongly delayed, with ossification centers being present in only 4 ± 1 of the coccygeal vertebrae in *VEGF*$^{188/188}$ mice compared with 14 ± 1 in WT at P1.5 ($P < 0.001$, $n = 8$) (Figure 1d). Metacarpals, metatarsals, and phalanges showed smaller ossified

centers, and the ossification in the calcaneus and talus was incomplete (Figure 1, e and f). The overall size of the long bones was decreased (Figure 1, e and f), and the ratio of proximal cartilage length to ossified diaphysis length was increased in *VEGF*$^{188/188}$ tibias compared with WT tibias at P1.5 (27% versus 16%, respectively; $P < 0.001$, $n = 8$) and P5 (not shown). In this study, we focused on long bone development.

Epiphyseal cartilage abnormalities in VEGF$^{188/188}$ *mice*. A severe delay in development of long bones was observed at E16.5, since the length of the primitive bone marrow cavity was reduced 80% ($P < 0.0001$; Supplementary Figure 1, b and c, http://www.jci.org/cgi/content/full/113/2/188/DC1), but chondrocyte morphology was normal. The cartilage of proximal and distal *VEGF*$^{188/188}$ tibias and femurs was clearly abnormal from E18.5 onwards, however. Initially, the morphology of the most centrally localized resting periarticular and prehypertrophic chondrocytes was altered, and this phenotype subsequently expanded to the entire length of the epiphysis at P1.5 (Figure 1g). By P5, the interior cartilage displayed a large hypocellular gap, extending from the articular region to the metaphyseal bone area (Figure 1h). Epiphyseal chondrocyte hypertrophy and invasion of vascular canals appeared in WT but not *VEGF*$^{188/188}$ mice. At P14, the formation of the secondary ossification center was severely delayed in *VEGF*$^{188/188}$ mice as compared with WT controls, and cartilage resorption was initiated only on the anterior side and progressed in unilateral direction instead of a bidirectional one (Figure 1i). Knee joint development was also consistently affected in all the mutants, with massive overgrowth and disorientation of synovial tissue and failure to form normal cruciate ligaments. Additionally, a diffuse transition zone instead of a well-defined boundary between articular surfaces and joint tissue was markedly evident at P28 (Figure 1j). It is noteworthy that chondrocytes in metatarsals at all ages appeared normal, whereas in tibias and femurs the severity of the cartilage lesion increased with the size of the epiphysis (not shown). Thus, epiphyseal chondrocyte development and secondary ossification center and knee joint formation were severely affected in *VEGF*$^{188/188}$ mice. In contrast, *VEGF*$^{164/164}$ mice had normal cartilage (not shown).

Apoptosis in the center of VEGF$^{188/188}$ *epiphyseal cartilage*. The morphologically altered central cartilage region in long bones of *VEGF*$^{188/188}$ mice contained collagen type II–rich matrix, as shown by immunohistochemistry on P1.5 hind limbs (Figure 2a). In situ hybridization of collagen type II or X could, however, not detect expression of these genes within the central region (Figure 2c), suggesting that this area contained quiescent or dead cells. TUNEL analysis revealed massive apoptosis in the central part of the resting/periarticular and proliferating/columnar chondrocyte zones of *VEGF*$^{188/188}$ neonates, whereas in WT cartilage only a few terminal hypertrophic chondrocytes were TUNEL positive (Figure 2b). Consistent with the temporally and spatially restricted occurrence of morphological alterations in

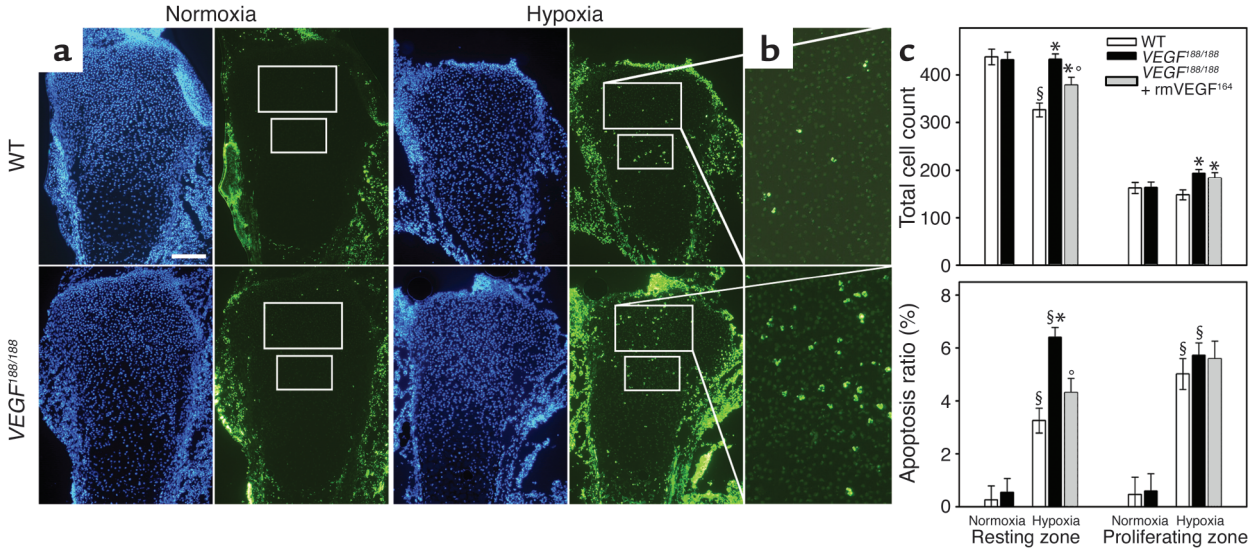

Figure 3
Altered response of *VEGF*$^{188/188}$ chondrocytes to hypoxia. Hind limbs from WT and *VEGF*$^{188/188}$ embryos were cultured in normoxia (21% O_2) or hypoxia (0.5% O_2) for 48 hours. (**a**) Sections were stained with TUNEL (green) and DAPI (blue). Measurements were performed in fixed areas in the resting and proliferating chondrocyte zones, as indicated. Scale bar: 150 μm. (**b**) Magnified view of TUNEL-stained resting chondrocyte zone of limbs cultured in hypoxia (turned 90° clockwise). (**c**) Quantification of total cell number and percentage of apoptotic cells (of total cell number) showing lack of growth inhibition in hypoxia and increased hypoxia-induced apoptosis in the resting chondrocyte zone of *VEGF*$^{188/188}$ limbs as compared with WT; $n = 4–5$; significant differences are $^{\S}P < 0.05$ versus normoxia of the same genotype (effect of condition); $^{*}P < 0.05$ versus WT in the same condition (effect of genotype). These effects could be partially or completely rescued, respectively, by supplementation of $rmVEGF_{164}$ to the mutant limbs ($n = 4–5$; $^{*}P < 0.05$ versus WT and $^{\circ}P < 0.05$ versus *VEGF*$^{188/188}$ in the same condition (effect of supplementation).

Table 1
Quantitative RT-PCR analysis of effect of hypoxia on expression of VEGF (isoforms), VEGF receptors, and HIFs in cultured embryonic hind limbs and primary chondrocytes

Gene[A]	HL normoxia	HL hypoxia[B]	PC normoxia	PC hypoxia[B]
Total VEGF	2,241 ± 160	6,581 ± 248[C]	102 ± 15	143 ± 11[D]
$VEGF_{120}$	899 ± 61	2,606 ± 200[C]	43 ± 4	73 ± 4[C]
$VEGF_{164}$	493 ± 19	1,407 ± 109[C]	29 ± 2	47 ± 3[C]
$VEGF_{188}$	178 ± 21	497 ± 30[C]	6.6 ± 0.5	12.5 ± 0.8[C]
NRP-1	184 ± 21	137 ± 15[E]	13 ± 1	11 ± 1[E]
Flt-1	10.5 ± 1.6	11.1 ± 1.1[E]	0.03 ± 0.01	0.04 ± 0.01[E]
Flk-1	24.2 ± 2.1	10.9 ± 0.3[C]	0.04 ± 0.01	0.05 ± 0.01[E]
HIF-1α	296 ± 45	200 ± 29[E]	189 ± 16	185 ± 12[E]
HIF-2α	25 ± 5	29 ± 7[E]	12 ± 2	14 ± 1[E]

[A]mRNA copy number of the indicated gene per 1,000 copies of *HPRT* mRNA. [B]*P* value for hypoxia versus normoxia. [C]$P < 0.001$; [D]$P < 0.05$; [E]NS. HL, hind limbs; PC, primary chondrocytes.

the cartilage of $VEGF^{188/188}$ mice, only a few apoptotic chondrocytes were detected centrally in E18.5 tibia and femur, whereas E16.5 growth plates and peripheral cartilage regions at all ages examined were devoid of apoptotic chondrocytes (not shown).

Increased hypoxia in $VEGF^{188/188}$ epiphyseal cartilage. The centrally restricted chondrocyte apoptosis in perinatal $VEGF^{188/188}$ mice might be explained by increased hypoxia, which was addressed by EF5 binding. This technique is based upon the hypoxia-dependent bioreduction of the nitroimidazole EF5, leading to binding of EF5 to cellular macromolecules. The distribution of these EF5-binding adducts is then detected with a fluorochrome-conjugated Ab. As shown previously (2), the interior of WT epiphyseal cartilage is hypoxic, as detected by prominent EF5 binding in the center of proliferating and prehypertrophic regions (Figure 2d). In $VEGF^{188/188}$ epiphyses, the staining intensity was apparently increased, and a second ectopic center of hypoxia was evident in the resting chondrocyte zone.

Examination of younger embryos showed that increased hypoxia preceded apoptosis in $VEGF^{188/188}$ epiphyses. At E16.5 no obvious morphological alterations and no TUNEL-positive cells were detected within the epiphyseal cartilage, yet EF5 staining was already increased and ectopically seen in the resting chondrocytes. The signal also extended deeply into the developing joint (Figure 2e), and in this area, a small cluster of apoptotic cells was detected at the interface between articular ligament tissues and periarticular chondrocytes in all the $VEGF^{188/188}$ embryos ($n = 6$) (Figure 2f), but not in WT mice.

Impaired epiphyseal cartilage vascularization in $VEGF^{188/188}$ mice. Tissue hypoxia is strongly linked to insufficient vascularization (4). Cartilage itself is avascular, and its vascular supply depends on metaphyseal vessels invading the hypertrophic chondrocyte zone and an elaborate vascular network overlying the epiphyseal cartilage. The density, pattern, and morphology of the vessels immediately lining the condylar epiphyseal cartilage of the distal femur was studied after angiography at P1.5 (Figure 2g). The epiphyseal capillary network around $VEGF^{188/188}$ cartilage was strongly impaired (Figure 2h), as evidenced by the significantly reduced vascularized area (Figure 2i), most likely resulting from a decrease in both vessel density and diameter. In addition, vessels at the rim of the femur condyle lining the avascular patellar face were oriented rather randomly as opposed to the strictly delineated orientation of vessels in WT mice (Figure 2h).

In contrast, no abnormalities were found in metaphyseal vascularization of P1.5 $VEGF^{188/188}$ tibias (see Supplementary Table 1, http://www.jci.org/cgi/content/full/113/2/188/DC1), and bone mineralization and resorption parameters were normal (see Supplementary Table 1, http://www.jci.org/cgi/content/full/113/2/188/DC1). Similarly, metaphyseal vascularization and mineralization were normal in $VEGF^{164/164}$ mice at P1.5 (not shown).

Thus, the combined absence of $VEGF_{120}$ and $VEGF_{164}$ in $VEGF^{188/188}$ mice did not affect metaphyseal vascularization but resulted in an impaired vascular network surrounding the epiphyseal cartilage, most likely causing the increased hypoxia.

$VEGF_{188}$ is insufficient to protect resting chondrocytes from hypoxia-induced apoptosis in vitro. In addition to its angiogenic properties, VEGF has also been described as a survival factor for some cell types (5). We therefore investigated in vitro whether the lack of the $VEGF_{120}$ and $VEGF_{164}$ isoforms may directly affect the apoptotic response of chondrocytes to hypoxia. Culturing WT embryonic hind limbs in hypoxic conditions induced apoptosis, as evidenced by a significantly decreased ratio of Bcl-2/Bax mRNA expression (Bcl-2/Bax mRNA copy number was 129 ± 15 in hypoxia versus 217 ± 22 in normoxia; $P = 0.01$; $n = 5$) and an increased number of TUNEL-positive cells as compared with normoxia (Figure 3a). In $VEGF^{188/188}$ limbs, the induction of apoptosis by hypoxia was significantly higher than in WT limbs, specifically in the resting chondrocyte zone (Figure 3, b and c). This effect could be completely reversed by addition of $rmVEGF_{164}$ to limb explants from $VEGF^{188/188}$ mice (Figure 3c).

Hypoxic stress significantly reduced the total cell count in the resting chondrocyte area in WT but not in *VEGF*$^{188/188}$ limbs, suggesting lack of growth inhibition in the mutants (Figure 3c). This was confirmed by staining for the proliferation marker KI67: WT limb explants showed significantly reduced proliferation (determined as the ratio of KI67-positive cells relative to DAPI-positive cells) when cultured in hypoxia as compared with normoxia, the reduction being 66% in resting chondrocytes (n = 4–5; P < 0.001). This growth inhibition response to hypoxia was completely lacking in *VEGF*$^{188/188}$ resting chondrocytes but was partially rescued by adding rmVEGF$_{164}$ (Figure 3c).

These findings indicate that, compared with WT cartilage, resting chondrocytes in *VEGF*$^{188/188}$ limbs are more susceptible to apoptosis and lack growth inhibition in hypoxic conditions. The rescue of this phenotype by rmVEGF$_{164}$ is in favor of a direct role for this isoform as a survival factor and growth regulator for hypoxic chondrocytes.

VEGF and NRP-1 are expressed by immature growth plate chondrocytes. The (angiogenic) activity of VEGF is tightly regulated by gene dosage (4). To exclude that *VEGF*$^{188/188}$ mice produced insufficient VEGF, its expression was quantified. VEGF$_{188}$ mRNA contributed minimally to the total VEGF mRNA level in WT femurs but was highly upregulated in *VEGF*$^{188/188}$ mice, resulting in similar or even higher total VEGF levels compared with WT mice (Figure 4a). High VEGF expression was localized in hypertrophic chondrocytes, as shown by in situ hybridization, but VEGF was also expressed in the resting and proliferating zones in both genotypes at P1.5. Noticeably, VEGF expression was strongly upregulated in *VEGF*$^{188/188}$ cartilage around the central lesion at P1.5 (Figure 4b) and near the articular ends in E16.5 limbs (Figure 4c), the regions of ectopic EF5 staining (see Figure 2, d and e). This upregulation of VEGF$_{188}$ expression may thus have been caused by the increased hypoxia, since a major cellular response to hypoxia is increased VEGF expression, mediated by HIFs (25). Indeed, culturing WT embryonic limbs or primary chondrocytes in hypoxia significantly upregulated mRNA of the three VEGF isoforms, all to a similar extent (Table 1). This induction was not associated with alterations in HIF-1α or HIF-2α mRNA levels (Table 1), in agreement with hypoxia regulation of these factors by protein stabilization (25).

Analysis of VEGF receptor expression showed that NRP-1 mRNA was highly expressed at the cartilage/bone border and in the perichondrium/periosteum. A weaker but marked signal was also detected in the proliferating chondrocyte zone of both WT and *VEGF*$^{188/188}$ bones (Figure 4d). Analysis by qRT-PCR revealed no significant difference in NRP-1 levels between WT and *VEGF*$^{188/188}$ femurs (not shown). The expression patterns of Flt-1 and Flk-1 were similar in WT and *VEGF*$^{188/188}$ tibias, being most prominent at the cartilage/bone interface, within the bone marrow region, and in the perichondrial/periostal area (Figure 4, e and f). Primary chondrocytes expressed NRP-1, but not Flk-1 or Flt-1 mRNA (Table 1), consistent with the in vivo data. No effect of hypoxia was detected on either VEGF receptor mRNA expression in primary chondrocytes, whereas cultured limbs showed moderate downregulation of Flk-1, and NRP-1 and Flt-1 levels remained unchanged (Table 1).

These data indicate that *VEGF*$^{188/188}$ mice have no deficit in the level of VEGF or VEGF receptors and that hypoxia comparably induces mRNA expression of the three VEGF isoforms in embryonic limbs and primary chondrocytes.

VEGF$^{188/188}$ *cartilage exhibits increased proliferation and decreased differentiation.* In contrast to the central lesion of *VEGF*$^{188/188}$ epiphyseal cartilage, the peripheral regions were devoid of morphological abnormalities. The ratio

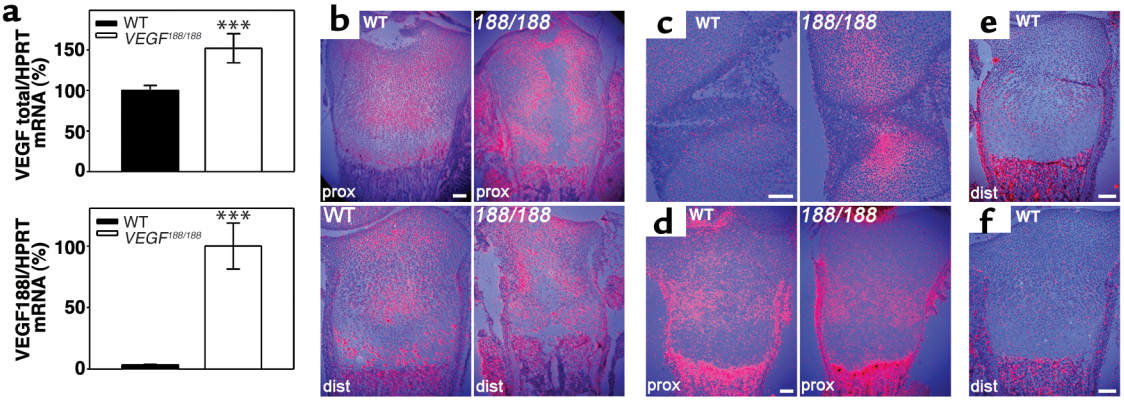

Figure 4
VEGF and VEGF receptor expression. (**a**) Total VEGF and VEGF$_{188}$ mRNA expression levels in P1.5 WT and *VEGF*$^{188/188}$ femurs were determined by qRT-PCR (n = 12; ***P < 0.001). The total VEGF level of WT mice and the VEGF$_{188}$ level of *VEGF*$^{188/188}$ mice were set at 100%. (**b** and **c**) In situ hybridization for VEGF showing (**b**) P1.5 proximal (prox) and distal (dist) tibia and (**c**) the knee joint region at E16.5. VEGF mRNA is detected in both hypertrophic and immature chondrocytes. Note increased VEGF expression in *VEGF*$^{188/188}$ epiphyses in regions of enhanced EF5 binding (see Figure 2). (**d**–**f**) In situ hybridization for the VEGF receptors (**d**) NRP-1, (**e**) Flk-1, and (**f**) Flt-1, in P1.5 tibia. (**d**) NRP-1 is expressed in the proliferating chondrocyte zone, as evident on WT and peripheral *VEGF*$^{188/188}$ sections through proximal tibia. (**e** and **f**) Flk-1 and Flt-1 show no detectable expression within the cartilage of WT tibia. Scale bars: 100 μm. *188/188*, *VEGF*$^{188/188}$.

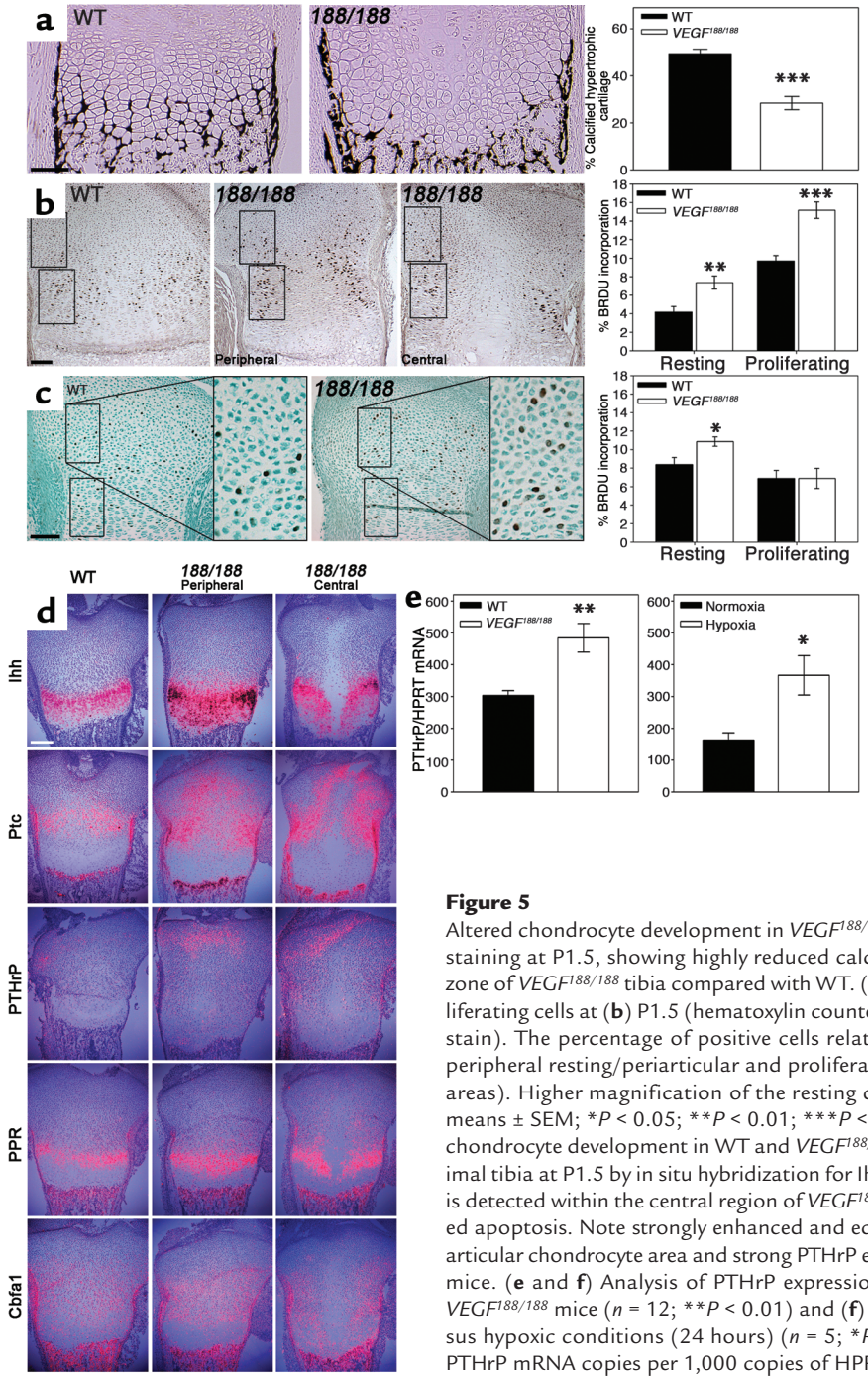

Figure 5

Altered chondrocyte development in *VEGF*$^{188/188}$ peripheral growth plates. (**a**) Von Kossa staining at P1.5, showing highly reduced calcification in the hypertrophic chondrocyte zone of *VEGF*$^{188/188}$ tibia compared with WT. (**b** and **c**) BrdU incorporation to detect proliferating cells at (**b**) P1.5 (hematoxylin counterstain) and (**c**) E16.5 (light green counterstain). The percentage of positive cells relative to total cell count was determined in peripheral resting/periarticular and proliferating/columnar zones, as indicated (boxed areas). Higher magnification of the resting chondrocyte area is shown (**c**). Values are means ± SEM; **P* < 0.05; ***P* < 0.01; ****P* < 0.001 (*n* = 5–8). (**d**) Molecular analysis of chondrocyte development in WT and *VEGF*$^{188/188}$ peripheral and central sections of proximal tibia at P1.5 by in situ hybridization for Ihh, Ptc, PTHrP, PPR, and Cbfa-1. No signal is detected within the central region of *VEGF*$^{188/188}$ bones, consistent with the documented apoptosis. Note strongly enhanced and ectopic expression of Ptc in the resting/periarticular chondrocyte area and strong PTHrP expression near the bone ends of *VEGF*$^{188/188}$ mice. (**e** and **f**) Analysis of PTHrP expression level by qRT-PCR on (**e**) P1.5 WT and *VEGF*$^{188/188}$ mice (*n* = 12; ***P* < 0.01) and (**f**) E16.5 WT limbs cultured in normoxic versus hypoxic conditions (24 hours) (*n* = 5; **P* < 0.05). Values represent the number of PTHrP mRNA copies per 1,000 copies of HPRT. Scale bars: (**a**–**c**) 100 μm; (**d**) 200 μm.

of hypertrophic to nonhypertrophic cartilage zones was significantly decreased 15% ($P < 0.05$). However, the ratio of cartilage calcification was severely reduced (Figure 5a), indicating decreased chondrocyte differentiation.

The chondrocyte proliferation rate, assessed by BrdU incorporation in P1.5 tibias, was significantly increased in the peripheral regions of *VEGF*$^{188/188}$ versus WT epiphyses, both in the resting and proliferating zones (Figure 5b), thus in or near the regions of increased hypoxia (see Figure 2d). This alteration in chondrocyte proliferation rate was not secondary to the apoptosis in the central area. Indeed, *VEGF*$^{188/188}$ mice already showed significantly increased chondrocyte proliferation at E16.5, specifically in the resting zone (Figure 5c), thus preceding the appearance of apoptosis in this area (see Figure 2f, arrowhead). The resting zone at E16.5 did, however, already show increased hypoxia (see Figure 2e, arrowhead). These in vivo data are in line with the in vitro results showing lack of growth inhibition in hypoxic *VEGF*$^{188/188}$ hind limbs.

Molecular analysis of chondrocyte differentiation. The abnormal chondrocyte development in P1.5 *VEGF*$^{188/188}$ epiphyseal cartilage was further investigated at the molecular level by in situ hybridization and qRT-PCR.

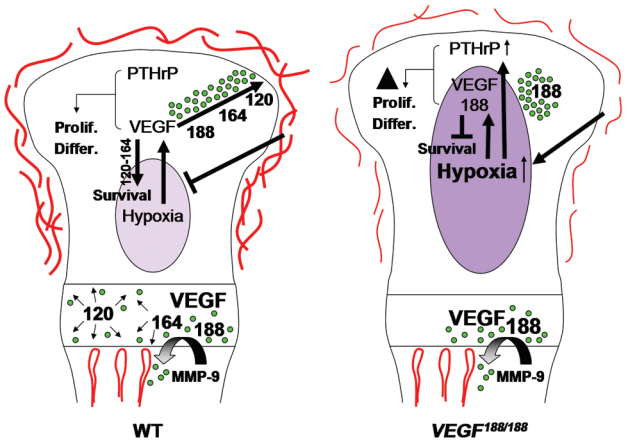

Figure 6
Proposed model of VEGF action in cartilage. VEGF is produced at high levels by hypertrophic chondrocytes where the longer VEGF isoforms become sequestered in the cartilage matrix. Proteases mediating cartilage resorption, such as MMP-9, release bound VEGF that acts upon endothelial cells, chondroclasts/osteoclasts, and osteoblasts, thereby coupling metaphyseal vascularization, cartilage resorption, and bone formation. When the epiphyseal cartilage exceeds a critical size during development, the midst of the growth plate becomes hypoxic, triggering VEGF expression in immature chondrocytes. Soluble VEGF isoforms are critical to diffuse to the perichondrium and stimulate outgrowth of the epiphyseal vascular network and subsequent vascular invasion preceding secondary ossification. In addition, VEGF also regulates chondrocyte development and survival. The $VEGF_{188}$ isoform is insufficient for these functions, due to restricted diffusion capacities and possibly to lack of interaction with NRP-1. Prolif., proliferation; Differ., differentiation.

In the central area of *VEGF*$^{188/188}$ cartilage, we could not detect the expression of any gene mentioned below, conforming to the finding of chondrocyte apoptosis in this region (see Figure 2b). Peripherally, the mRNA expression pattern of the chondrocyte regulatory factor Ihh seemed normal (Figure 5d), with Ihh being expressed predominantly by prehypertrophic chondrocytes as in WT tibias. Ihh mRNA levels were not significantly altered in *VEGF*$^{188/188}$ femurs as compared with WT (not shown). Similarly, PPR and Cbfa-1 expression patterns (Figure 5d) and levels (not shown) were apparently normal at the periphery of *VEGF*$^{188/188}$ growth plates.

On the other hand, Ptc, an Ihh receptor and transcriptional target, was strongly upregulated and ectopically expressed in the periarticular cartilage region and the area surrounding the lesion in *VEGF*$^{188/188}$ mice, as seen on both central and peripheral sections. In WT growth plates, Ptc mRNA was expressed most strongly in columnar proliferating chondrocytes close to Ihh-expressing prehypertrophic chondrocytes, with its expression decreasing toward the articular end of the bone. In both genotypes, Ptc mRNA was also localized in the perichondrium adjacent to the prehypertrophic zone and at the cartilage/bone interface in the primary spongiosa (Figure 5d).

Ectopic Ptc expression in *VEGF*$^{188/188}$ cartilage was associated with increased PTHrP mRNA near the articular surface (Figure 5d). Analysis by qRT-PCR demonstrated 60% increased PTHrP expression in femurs of *VEGF*$^{188/188}$ mice as compared with WT ($P < 0.01$) (Figure 5e). It is noteworthy that hypoxia also significantly induced PTHrP mRNA expression more than twofold in WT embryonic limbs as compared with normoxia ($P < 0.05$) (Figure 5e).

Thus, the periphery of neonatal *VEGF*$^{188/188}$ growth plates showed increased chondrocyte proliferation and decreased differentiation associated with disturbed expression of genes involved in the Ihh-PTHrP pathway that controls the pace of chondrocyte maturation.

Discussion

To explore the role of the VEGF isoforms in endochondral bone development, we studied this process in mice expressing single VEGF isoforms. Our data suggest that different molecular processes regulate epiphyseal and metaphyseal vascularization and indicate a role for VEGF in chondrocyte development and survival.

Soluble VEGF isoforms are essential for epiphyseal vascularization and secondary ossification. In this study, we provide new insights in the mechanisms controlling the development and growth of long bones. Epiphyseal cartilage is avascular, and its oxygenation is critically dependent on the surrounding vessels. The angiogenic factors responsible for epiphyseal vascularization were elusive, but the present study implicates VEGF in this process. VEGF exists as three isoforms: a soluble $VEGF_{120}$, a matrix-bound $VEGF_{188}$, and $VEGF_{164}$, which can both diffuse and bind matrix and interacts with the receptor NRP-1 (5). Mice lacking $VEGF_{120}$ and $VEGF_{164}$, leaving expression of only $VEGF_{188}$, displayed abnormalities in the capillary network overlying the epiphyses, associated with increased hypoxia and massive cell death in the interior of the cartilage. A likely explanation is that the presence of $VEGF_{188}$ only is insufficient to establish epiphyseal vascularization since this isoform binds tightly to matrix components and cellular surfaces, thereby failing to diffuse toward the perichondrium. Although VEGF isoform-specific signaling cannot be excluded, an argument favoring the diffusion hypothesis is provided by our observation that mice expressing either $VEGF_{164}$ or $VEGF_{120}$, in addition to $VEGF_{188}$ (*VEGF*$^{164/188}$ and *VEGF*$^{120/188}$ mice, respectively), show no evidence of defects in epiphyseal vascularization (see Supplementary Figure 2, http://www.jci.org/cgi/content/full/113/2/188/DC1. Also, the phenotype of mice with inactivation of *HIF-1α* in cartilage (2) is consistent with this hypothesis. In this mouse model, chondrocytes located in the central part of the growth plate underwent apoptosis, and despite the HIF-1α deficiency, VEGF expression was increased in immature cartilage resulting in ectopic angiogenesis. Centrally localized apoptosis is also seen in epiphyseal cartilage of *VEGF*$^{188/188}$ mice, as well as high expression of VEGF, yet the ectopic vascular invasion is not observed, suggesting that soluble VEGF isoforms are required to attract epiphyseal vessels. Additionally, chondrocyte

apoptosis in hind limbs of *VEGF*$^{188/188}$ mice only became apparent at perinatal ages, and severity of the lesion was coupled to bone size, data that are compatible with the need for soluble isoforms.

As development progresses, nutrition and oxygenation of the epiphysis by diffusion from surrounding vessels becomes insufficient, and vascular canals containing blood vessels and mesenchymal cells invade the cartilage (13–15). Both the initial vascular invasion and the subsequent development of the secondary ossification center were impaired in *VEGF*$^{188/188}$ mice. These processes were also disrupted in MT1-MMP–deficient mice (16, 17), suggesting that invasion may depend on the proteolytic activity of MT1-MMP to degrade the uncalcified matrix and on the angiogenic activity of VEGF to attract vessels.

Thus, our data suggest that progressive growth of normal avascular epiphyseal cartilage results in a state of increasing hypoxia, inducing VEGF expression. Soluble VEGF isoforms diffuse from the hypoxic center toward the periphery, thereby stimulating epiphyseal vessel outgrowth and thus reducing hypoxic stress (Figure 6). Later, VEGF induces invasion of vessels into the cartilage, initiating secondary ossification.

Longitudinal growth has been suggested to depend largely on an adequate epiphyseal circulation (18, 26), an observation consistent with the reduced growth of long bones in *VEGF*$^{188/188}$ mice. The abnormal development of the knee joint in *VEGF*$^{188/188}$ mice was also most likely related to the defective vascularization, since aberrant hypoxia in the articular region was detected already at an early stage. The mice used in this study did not seem to suffer from significant physiological problems other than the dwarfism and joint pathology described here. This may indicate that cartilage, being an avascular tissue of considerable size during development, is particularly vulnerable to even moderate alterations in vascularization and consequently in nutrient and oxygen supply. Although highly speculative at present, this may be an interesting link to pediatric orthopedics including osteo- or chondronecrosis or to some types of yet unexplained dwarfisms and/or known chondrodysplasias, which may include an angiogenic component in modulating disease severity.

Matrix-bound VEGF isoforms are required for metaphyseal vascularization. Interestingly, the metaphyseal vasculature was normal in both *VEGF*$^{188/188}$ and *VEGF*$^{164/164}$ mice. In contrast, severely impaired metaphyseal angiogenesis, associated with an enlarged hypertrophic chondrocyte zone and impaired trabecular bone formation, has been reported in mice expressing only $VEGF_{120}$ (9, 10), in models of inactivation of all VEGF isoforms, either temporally (8) or locally (27), and when insufficient angiogenic factors (including VEGF) were released from the chondrocyte matrix due to MMP-9 deficiency (28). Taken together, these studies suggest that the release of VEGF isoforms from the chondrocyte matrix is necessary and sufficient for metaphyseal vascularization and that binding of VEGF to extracellular matrix favors organized angiogenesis, possibly by establishing a VEGF gradient. It is noteworthy that early embryonic bone development is retarded in *VEGF*$^{188/188}$ as well as *VEGF*$^{120/120}$ (9) mice, supporting the hypothesis that a gradient of soluble and bound VEGF molecules may be needed to coordinate initial capillary invasion and cartilage remodeling. On the other hand, the differential functioning of the VEGF isoforms may suggest that signaling through NRP-1, binding only $VEGF_{164}$, is important for bone development (see below). However, the possible role of a VEGF gradient and of NRP-1 in bone development remains to be further investigated.

VEGF directly affects chondrocyte development and survival in hypoxic cartilage. Increased proliferation and apoptosis of chondrocytes in *VEGF*$^{188/188}$ mice apparently colocalized with aberrant hypoxia, suggesting reduced oxygen tension to be the causal mechanism. In addition to the vascular defects upon *VEGF*$^{188/188}$ cartilage, however, our data also indicated a direct function of VEGF in hypoxic chondrocytes.

VEGF effect on chondrocyte development and survival. During development, cartilage inherently becomes hypoxic, but chondrocytes are well capable of surviving this challenge. In general, hypoxia induces the expression of genes involved in glucose metabolism and angiogenesis, including VEGF, via the transcriptional regulators HIF-1α and HIF-2α (25). In agreement, our data show that VEGF mRNA levels (all isoforms) were increased by hypoxia in both embryonic limbs and primary chondrocytes (ref. 1 and the present study). Noticeably, *VEGF*$^{188/188}$ embryonic limbs cultured in hypoxic conditions expressed amounts of total VEGF mRNA similar to WT limbs (data not shown). The mutant limbs, however, showed increased chondrocyte apoptosis in hypoxia compared with WT controls, which could be rescued by supplementing $rmVEGF_{164}$. Thus, the expression of $VEGF_{188}$ only was insufficient to protect chondrocytes against hypoxia-induced apoptosis, likely due to absence of $VEGF_{164}$. An important role for the $VEGF_{120}$ isoform in the survival of hypoxic chondrocytes is less probable, as 10-day-old mice coexpressing $VEGF_{120}$ and $VEGF_{188}$ (*VEGF*$^{120/188}$ mice) showed a centrally located abnormal epiphyseal region at a site that becomes substantially hypoxic during normal development, consistent with decreased chondrocyte survival in these mice (see Supplementary Figure 2, http://www.jci.org/cgi/content/full/113/2/188/DC1). This suggests that specific VEGF isoforms play a role in chondrocyte survival, a function recently also ascribed to HIF-1α (2). The role of VEGF as a survival factor is well established for endothelial cells (29), but has also been reported for hematopoietic stem cells (30), neuronal cells (31), osteoclasts (32), and several types of tumors (33, 34).

Immature chondrocyte cell death was not previously described in models of VEGF inactivation (8, 27), probably because of age differences or residual expression of the various isoforms. In the study by Haigh et al. (27)

embryonic death in the heterozygous state precluded investigation of older and/or homozygous animals, whereas Gerber et al. (8) inactivated VEGF in juvenile mice, bypassing development.

The increased hypoxia was also associated with altered proliferation/differentiation balance in *VEGF$^{188/188}$* mice. This morphological finding agrees with the observed upregulation of Ptc and PTHrP mRNA (35). The observation that hypoxia induced PTHrP expression in cultured limbs suggests that the altered gene expression and chondrocyte development may have resulted from the ectopically increased hypoxia in *VEGF$^{188/188}$* cartilage. Alternatively, it may represent a direct role of VEGF, as suggested by our in vitro experiments (Figure 6). Noticeably, increased chondrocyte proliferation preceded apoptosis, suggesting it was not a compensatory mechanism.

Signaling through NRP-1? VEGF and the $VEGF_{164}$-receptor NRP-1 are expressed in epiphyseal chondrocytes in vivo and in vitro, suggesting a role for $VEGF_{164}$ in regulating cartilage development. Interestingly, cartilage and bone development were affected by overexpression of NRP-1 (36) or inactivation of semaphorin-3A (37), a NRP-1 ligand that may compete with $VEGF_{165}$ (the human isoforms contain one amino acid more than the murine proteins) (38, 39). Studies on NRP-1 function highlighted its role as a coreceptor for Flk-1, enhancing binding and bioactivity of $VEGF_{165}$ (7, 40). Bachelder et al. (33), however, identified an autocrine survival role of $VEGF_{165}$, but not $VEGF_{121}$, on breast carcinoma cells expressing NRP-1 only. Possibly, NRP-1 may transduce VEGF signaling alone or in concert with other (yet unidentified) receptors in some cell types. On the other hand, very low levels of Flk-1 expression in chondrocytes cannot be excluded in our study.

In conclusion, we showed that mice expressing exclusively the $VEGF_{188}$ isoform exhibited massive apoptosis and impaired maturation of chondrocytes, dwarfism, and severe joint dysplasia. This phenotype was due to epiphyseal vascular alterations causing increased hypoxia, combined with lack of VEGF isoform-specific signaling in the growth plate (see Figure 6). These findings are the first to shed light on the angiogenic control of epiphyseal vascularization and secondary ossification and to identify VEGF as a key regulator of this process. It is noteworthy that the expression of only $VEGF_{164}$ in mice was sufficient for normal bone and cartilage development. In a previous study we showed that expression of only $VEGF_{120}$ impaired metaphyseal vascularization and endochondral ossification (9). Thus, different molecular processes requiring specific VEGF isoforms regulate epiphyseal and metaphyseal vascularization during bone development. The matrix-bound VEGF isoforms are essential in the metaphysis, whereas the soluble isoforms are crucial for epiphyseal development. In addition, the VEGF isoforms differ in their capability to regulate proliferation and survival of chondrocytes in hypoxic conditions. We conclude that the integrated actions of the three VEGF isoforms are essential to couple metaphyseal and epiphyseal vascularization, cartilage morphogenesis, and ossification during endochondral bone development.

Acknowledgments

The authors thank S. Torrekens and S. Wyns for assistance. We are grateful to F. Luyten, H.M. Kronenberg, P. Ducy, U.I. Chung, C.J.M. de Vries, and J. Helms for the supply of in situ hybridization probes, to C. Koch and the National Cancer Institute for providing EF5 without charge, and to N. Mertens and D. Lambrechts for collaborating in providing $rmVEGF_{164}$. We express our gratitude to M. Tjwa and A. Bouché for sharing their expertise in angiography and to E. Daci for advising on BrdU labeling. B. Hassan, F. Luyten, and P. Tylzanowski are acknowledged for sharing equipment and expertise in imaging and for helpful discussions. We are also grateful to P. Tylzanowski for critically reading the manuscript. This work was supported by Fonds voor Wetenschappelijk Onderzoek (Belgium) grant G.0225.00 and a grant from Chugai. C. Maes is a fellow of the Instituut voor de aanmoediging van Innovatie door Wetenschap en Technologie in Vlaanderen. Due to space constraints, a number of important references could not be included in this article. Interested readers can find a supplementary reading list at http://www.jci.org/cgi/content/full/113/2/188/DC1.

1. Pfander, D., Cramer, T., Schipani, E., and Johnson, R.S. 2003. HIF-1α controls extracellular matrix synthesis by epiphyseal chondrocytes. *J. Cell Sci.* **116**:1819–1826.
2. Schipani, E., et al. 2001. Hypoxia in cartilage: HIF-1α is essential for chondrocyte growth arrest and survival. *Genes Dev.* **15**:2865–2876.
3. Karsenty, G., and Wagner, E.F. 2002. Reaching a genetic and molecular understanding of skeletal development. *Dev. Cell* **2**:389–406.
4. Carmeliet, P. 2000. Mechanisms of angiogenesis and arteriogenesis. *Nat. Med.* **6**:389–395.
5. Robinson, C.J., and Stringer, S.E. 2001. The splice variants of vascular endothelial growth factor (VEGF) and their receptors. *J. Cell Sci.* **114**:853–865.
6. Neufeld, G., et al. 2002. The neuropilins: multifunctional semaphorin and VEGF receptors that modulate axon guidance and angiogenesis. *Trends Cardiovasc. Med.* **12**:13–19.
7. Soker, S., Takashima, S., Miao, H.Q., Neufeld, G., and Klagsbrun, M. 1998. Neuropilin-1 is expressed by endothelial and tumor cells as an isoform-specific receptor for vascular endothelial growth factor. *Cell.* **92**:735–745.
8. Gerber, H.P., et al. 1999. VEGF couples hypertrophic cartilage remodeling, ossification and angiogenesis during endochondral bone formation. *Nat. Med.* **5**:623–628.
9. Maes, C., et al. 2002. Impaired angiogenesis and endochondral bone formation in mice lacking the vascular endothelial growth factor isoforms VEGF164 and VEGF188. *Mech. Dev.* **111**:61–73.
10. Zelzer, E., et al. 2002. Skeletal defects in VEGF(120/120) mice reveal multiple roles for VEGF in skeletogenesis. *Development.* **129**:1893–1904.
11. Brighton, C.T. 1978. Structure and function of the growth plate. *Clin. Orthop.* **136**:22–32.
12. Wirth, T., et al. 2002. The blood supply of the growth plate and the epiphysis: a comparative scanning electron microscopy and histological experimental study in growing sheep. *Calcif. Tissue Int.* **70**:312–319.
13. Cole, A.A., and Wezeman, F.H. 1985. Perivascular cells in cartilage canals of the developing mouse epiphysis. *Am. J. Anat.* **174**:119–129.
14. Floyd, W.E., Zaleske, D.J., Schiller, A.L., Trahan, C., and Mankin, H.J. 1987. Vascular events associated with the appearance of the secondary center of ossification in the murine distal femoral epiphysis. *J. Bone Joint Surg. Am.* **69**:185–190.
15. Rivas, R., and Shapiro, F. 2002. Structural stages in the development of the long bones and epiphyses: a study in the New Zealand white rabbit. *J. Bone Joint Surg. Am.* **84**:85–100.
16. Holmbeck, K., et al. 1999. MT1-MMP–deficient mice develop dwarfism,

osteopenia, arthritis, and connective tissue disease due to inadequate collagen turnover. *Cell.* **99**:81–92.
17. Zhou, Z., et al. 2000. Impaired endochondral ossification and angiogenesis in mice deficient in membrane-type matrix metalloproteinase I. *Proc. Natl. Acad. Sci. U. S. A.* **97**:4052–4057.
18. Brashear, H.R. 1963. Epiphyseal avascular necrosis and its relation to longitudinal bone growth. *J. Bone Joint Surg. Am.* **45-A**:1423–1438.
19. Trueta, J., and Amato, V.P. 1960. The vascular contribution to osteogenesis. III. Changes in the growth cartilage caused by experimentally induced ischaemia. *J. Bone Joint Surg. Br.* **42-B**:571–587.
20. Flanigan, D.P., Keifer, T.J., Schuler, J.J., Ryan, T.J., and Castronuovo, J.J. 1983. Experience with latrogenic pediatric vascular injuries. Incidence, etiology, management, and results. *Ann. Surg.* **198**:430–442.
21. Walter, P.K., and Hoffmann, W. 2000. Diminished epiphyseal growth following iatrogenic vascular trauma. *Eur. J. Vasc. Endovasc. Surg.* **20**:214–216.
22. Stalmans, I., et al. 2002. Arteriolar and venular patterning in retinas of mice selectively expressing VEGF isoforms. *J. Clin. Invest.* **109**:327–336. doi:10.1172/JCI200214362.
23. Ryan, H.E., Lo, J., and Johnson, R.S. 1998. HIF-1α is required for solid tumor formation and embryonic vascularization. *EMBO J.* **17**:3005–3015.
24. Amling, M., et al. 1997. Bcl-2 lies downstream of parathyroid hormone-related peptide in a signaling pathway that regulates chondrocyte maturation during skeletal development. *J. Cell Biol.* **136**:205–213.
25. Semenza, G.L. 2000. HIF-1: mediator of physiological and pathophysiological responses to hypoxia. *J. Appl. Physiol.* **88**:1474–1480.
26. Tomita, Y., et al. 1986. The role of the epiphyseal and metaphyseal circulations on longitudinal growth in the dog: an experimental study. *J. Hand Surg. [Am.].***11**:375–382.
27. Haigh, J.J., Gerber, H.P., Ferrara, N., and Wagner, E.F. 2000. Conditional inactivation of VEGF-A in areas of collagen2a1 expression results in embryonic lethality in the heterozygous state. *Development.* **127**:1445–1453.
28. Vu, T.H., et al. 1998. MMP-9/gelatinase B is a key regulator of growth plate angiogenesis and apoptosis of hypertrophic chondrocytes. *Cell.* **93**:411–422.
29. Zachary, I., and Gliki, G. 2001. Signaling transduction mechanisms mediating biological actions of the vascular endothelial growth factor family. *Cardiovasc. Res.* **49**:568–581.
30. Gerber, H.P., et al. 2002. VEGF regulates haematopoietic stem cell survival by an internal autocrine loop mechanism. *Nature.* **417**:954–958.
31. Oosthuyse, B., et al. 2001. Deletion of the hypoxia-response element in the vascular endothelial growth factor promoter causes motor neuron degeneration. *Nat. Genet.* **28**:131–138.
32. Nakagawa, M., et al. 2000. Vascular endothelial growth factor (VEGF) directly enhances osteoclastic bone resorption and survival of mature osteoclasts. *FEBS Lett.* **473**:161–164.
33. Bachelder, R.E., et al. 2001. Vascular endothelial growth factor is an autocrine survival factor for neuropilin-expressing breast carcinoma cells. *Cancer Res.* **61**:5736–5740.
34. Dias, S., Shmelkov, S.V., Lam, G., and Rafii, S. 2002. VEGF(165) promotes survival of leukemic cells by Hsp90-mediated induction of Bcl-2 expression and apoptosis inhibition. *Blood.* **99**:2532–2540.
35. Kronenberg, H.M. 2003. Developmental regulation of the growth plate. *Nature.* **423**:332–336.
36. Kitsukawa, T., Shimono, A., Kawakami, A., Kondoh, H., and Fujisawa, H. 1995. Overexpression of a membrane protein, neuropilin, in chimeric mice causes anomalies in the cardiovascular system, nervous system and limbs. *Development.* **121**:4309–4318.
37. Behar, O., Golden, J.A., Mashimo, H., Schoen, F.J., and Fishman, M.C. 1996. Semaphorin III is needed for normal patterning and growth of nerves, bones and heart. *Nature.* **383**:525–528.
38. Bagnard, D., et al. 2001. Semaphorin 3A-vascular endothelial growth factor-165 balance mediates migration and apoptosis of neural progenitor cells by the recruitment of shared receptor. *J. Neurosci.* **21**:3332–3341.
39. Miao, H.Q., et al. 1999. Neuropilin-1 mediates collapsin-1/semaphorin III inhibition of endothelial cell motility: functional competition of collapsin-1 and vascular endothelial growth factor-165. *J. Cell Biol.* **146**:233–242.
40. Soker, S., Miao, H.Q., Nomi, M., Takashima, S., and Klagsbrun, M. 2002. VEGF165 mediates formation of complexes containing VEGFR-2 and neuropilin-1 that enhance VEGF165-receptor binding. *J. Cell Biochem.* **85**:357–368.